Nearly three-dimensional Dirac fermions in an organic crystalline material unveiled by electron spin resonance

Ryuhei Oka, Keishi Ohara, Naoya Tajima, Toshihiro Shimada, and Toshio Naito

Electronic Supplementary Information

Experimental Details

The neutral ET was purchased from Tokyo Chemical Industry Co., Ltd. (TCI). The single crystals of α-ET_2I_3 were synthesised as reported.[S1] The electron spin resonance spectra of the X-band (~9.3 GHz) were measured on the single crystals of α-D_2I_3 in the temperature range 120-300 K using a JEOL JES-FA100. The single crystal was mounted on a Teflon piece settled with a minimal amount of Apiezon N grease, sealed in a 5 mm diameter quartz sample tube in a low-pressure (~ 20 mmHg) helium atmosphere. The *Q*-values, time constant, sweep time, modulation, and its amplitude were 4700-8200, 0.03 s, 1 min, 100 kHz, and 2 mT, respectively. The root dependence of the ESR intensities on the microwave power was checked for saturation and the power was selected to be 9 mW. The magnetic field was corrected by a gauss meter (JEOL NMR Field Meter ES-FC5) at the end of every measurement and was double-checked using a Mn(II) compound diluted in MgO powder as an external standard sample. The temperature was controlled using a continuous flow-type liquid N_2 cryostat with a digital temperature controller (JEOL) so as not to allow the temperature variation to exceed ± 0.5 K during the field sweep. The cooling rate was -10 K/min. Magnetic fields (***B***) are initially ($\theta = 0$) applied parallel to the *a*-axis for all the samples. In the measurements of anisotropy, the angle θ defines the rotation angle around the *b*-axis from the *a*-axis toward the *c*-axis. The temperature- and magnetic-filed-angular-dependencies were respectively examined using the same single crystal, and different crystals were examined for checking reproducibility and sample dependence. For detecting any artefact such as cracking of the crystals, the ESR spectra at 296 K and $\theta = 0$ were checked before and after the temperature- and magnetic-filed-angular-dependence measurements.

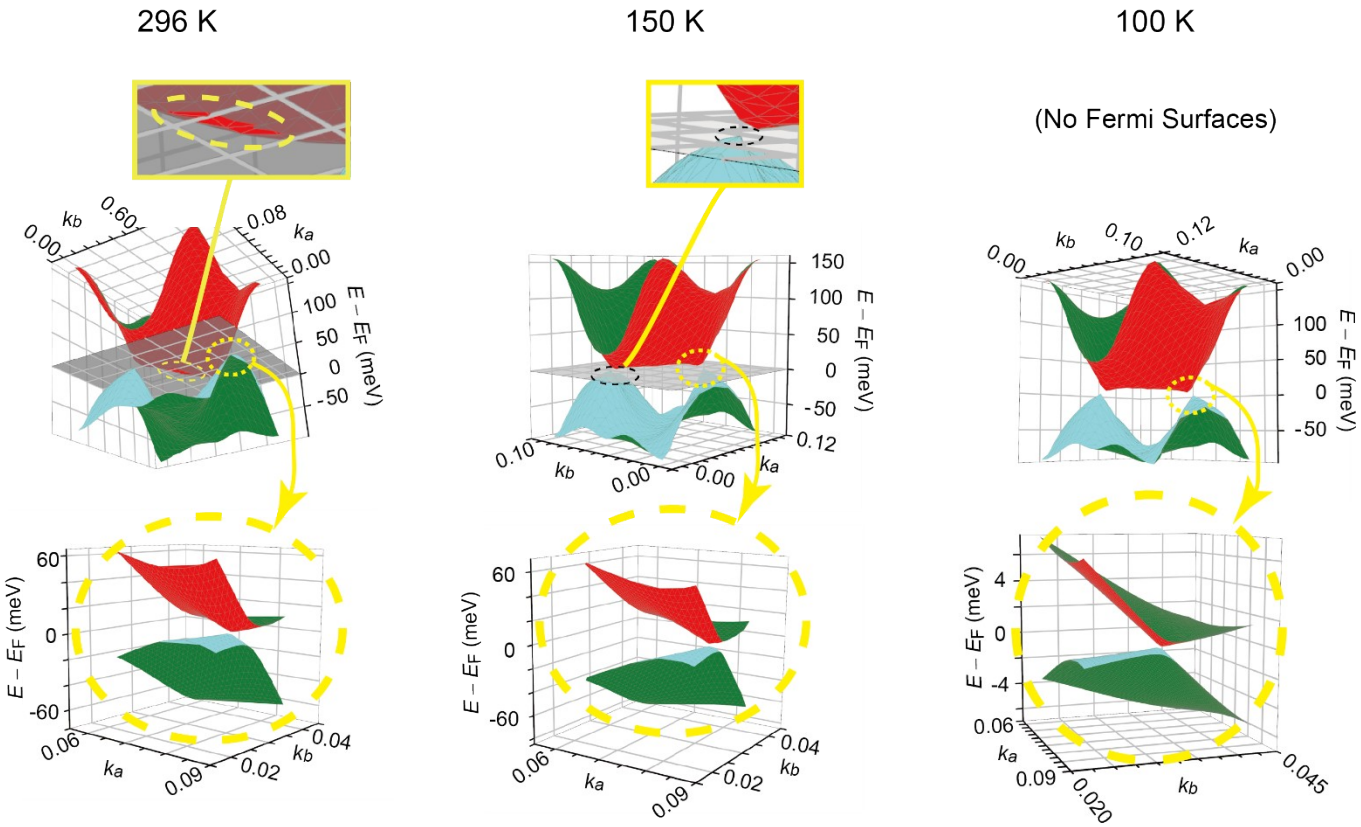

Fig. S1. Band structures near the Fermi level E_F in α-ET_2I_3 at 1 bar and 296, 150, and 100 K in the k_ak_b plane. At each T, (top) an enlarged view of the Fermi surfaces, (middle) an entire view with the Fermi level shown by the half-transparent grey plane, and (bottom) an enlarged view of developing Dirac cones. The red (front)/green (back) and blue (front)/green (back) curved surfaces respectively show a part of the top and the second HOMO bands. The energy separation between the Dirac points is ≤5–10 meV independent of T.

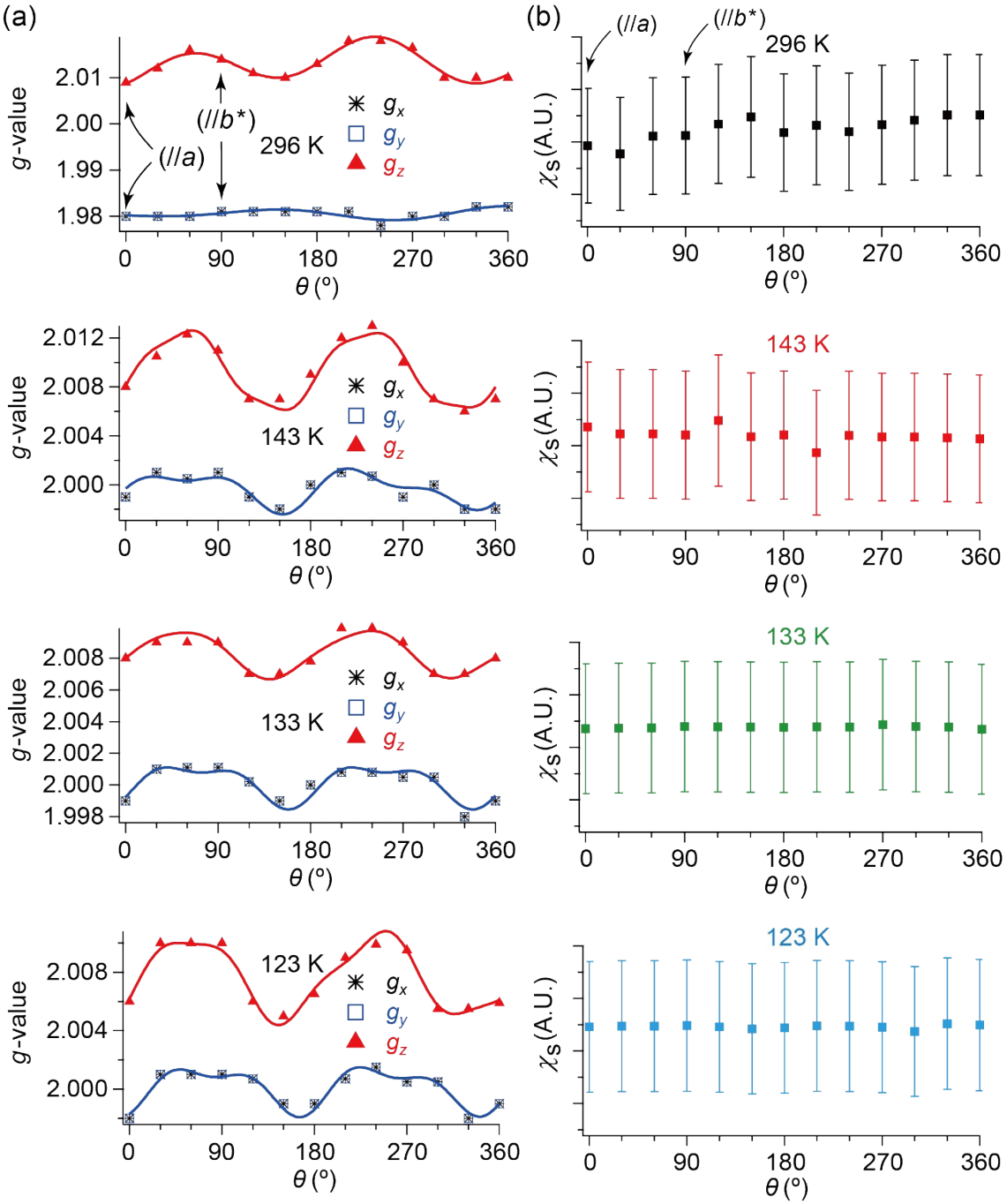

Fig. S2. θ- and T-dependencies in the ESR spectra of (**a**) g-values and (**b**) spin susceptibility χ_s when the single crystal was rotated around the c-axes. The susceptibility is shown in an arbitrary unit, as the absolute values were not estimated. The angle $\theta = 0°$ indicates that the applied magnetic field is parallel with the a-axis in both rotations. In all the panels, the data are derived from the simulation spectra and are shown with error bars (±10%). In each panel of (a), the curves indicate the best-fitting curves using Eq. 2. The obtained parameters are summarised in **Tables S1—S8**. Note that all g_x and g_y coincide with each other in each panel of (a). The subscripts x, y and z of the g-values approximately indicate the following directions: (x, y) ≈ (a, b) or (b, a), and $z \approx c$-axis. Whether (x, y) ≈ (a, b) or (b, a) could not be determined based on the ESR data. Although the unit of angle θ was radian in the fitting, it is described in degree in this figure.

Table S1. The parameters for reproducing the main peak at different magnetic-filed-angles (θ/°) for the *b*-axis rotation spectra at 296 K.*

θ/°	g_x	g_y	g_z	Γ_x	Γ_y	Γ_z
0	1.99	2	2.022	7	7	10
30	1.982	2.005	2.03	6.5	6	5.5
60	1.976	2.02	2.032	9.5	9	5.5
90	1.976	2.02	2.032	6	9	10.5
120	1.976	2.02	2.032	6	9	10.5
150	1.99	2.005	2.022	8	7	10
180	1.99	1.998	2.022	7	7	10
210	1.982	2.005	2.03	6.5	6	5.5
240	1.972	2.02	2.032	9.5	9	5.5
270	1.976	2.02	2.032	6	9	10.5
300	1.976	2.02	2.032	6	9	10.5
330	1.99	2.005	2.022	8	7	10
360	1.99	1.998	2.022	7	7	10

*Most of the simulated spectrum agreed well with the observed spectrum as shown in **Fig. 6c**.

Table S2. The parameters for reproducing the main peak at different magnetic-filed-angles (θ/°) for the *b*-axis rotation spectra at 143 K.*

θ/°	g_x	g_y	g_z	Γ_x (mT)	Γ_y (mT)	Γ_z (mT)
0	1.98	2.015	2.027	5	5	4
30	1.972	2	2.03	6.5	6	3.5
60	1.972	2.02	2.032	9.5	9	5.5
90	1.972	2.02	2.09	7.5	7	2.5
120	1.952	2.02	2.03	7.5	7	2.5
150	1.982	2.016	2.02	7	7	5
180	1.98	2.015	2.025	5	5	4
210	1.972	2	2.02	6.5	6	3.5
240	1.972	2.02	2.032	9.5	9	5.5
270	1.972	2.02	2.08	7.5	7	2.5
300	1.952	2.02	2.03	7.5	7	2.5
330	1.982	2.016	2.01	7	7	5
360	1.98	2.015	2.025	5	5	4

*Most of the simulated spectrum agreed well with the observed spectrum as shown in **Fig. 6c**.

Table S3. The parameters for reproducing the main peak at different magnetic-filed-angles (θ/°) for the *b*-axis rotation spectra at 133 K.*

θ/°	g_x	g_y	g_z	Γ_x (mT)	Γ_y (mT)	Γ_z (mT)
0	1.98	2.01	2.015	10	10	3
30	1.972	2	2.03	7.5	7	3.5
60	1.972	2.02	2.032	11.5	11	2
90	1.972	2.02	2.07	11.5	11	2.5
120	1.972	2.02	2.04	10.5	11	3
150	1.98	2.01	2.02	9	9	3
180	1.98	2.01	2.015	10	10	3
210	1.972	2	2.02	7.5	7	3.5
240	1.972	2.02	2.032	11.5	11	2
270	1.972	2.02	2.07	11.5	11	2.5
300	1.972	2.02	2.04	10.5	11	3
330	1.98	2.01	2.02	9	9	3
360	1.98	2.01	2.015	10	10	3

*Most of the simulated spectrum agreed well with the observed spectrum as shown in **Fig. 6c**.

Table S4. The parameters for reproducing the main peak at different magnetic-filed-angles (θ/°) for the *b*-axis rotation spectra at 123 K.*

θ/°	g_x	g_y	g_z	Γ_x (mT)	Γ_y (mT)	Γ_z (mT)
0	1.99	2.002	2.003	4	4	1.4
30	1.98	2.01	2.02	9	9	3
60	1.972	2.02	2.05	11.5	11	2
90	1.972	2.02	2.07	11.5	11	2.5
120	1.972	2.02	2.05	11.5	11	2.5
150	1.98	2.01	2.02	9	9	3
180	1.99	2.002	2.003	4	4	1.4
210	1.98	2.01	2.02	9	9	3
240	1.972	2.02	2.05	11.5	11	2
270	1.972	2.02	2.07	11.5	11	2.5
300	1.972	2.02	2.05	11.5	11	2.5
330	1.98	2.01	2.02	9	9	3
360	1.99	2.002	2.003	4	4	1.4

*Most of the simulated spectrum agreed well with the observed spectrum as shown in **Fig. 6c**.

Table S5. The parameters for reproducing the main peak at different magnetic-filed-angles (θ/°) for the *c*-axis rotation spectra at 296 K.*

θ/°	g_x	g_y	g_z	Γ_x (mT)	Γ_y (mT)	Γ_z (mT)
0	1.98	1.98	2.009	13	13	2.18
30	1.98	1.98	2.012	14.19	14.45	2.18
60	1.98	1.98	2.016	11.69	11.55	2.78
90	1.981	1.981	2.014	10.5	10.5	2.82
120	1.981	1.981	2.011	9.5	9.5	2.82
150	1.981	1.981	2.01	7	7	2.75
180	1.981	1.981	2.013	10	10	2.45
210	1.981	1.981	2.018	10	10	2.45
240	1.978	1.978	2.018	10	10	2.82
270	1.98	1.98	2.0165	10	10	2.82
300	1.98	1.98	2.01	9	9	2.82
330	1.982	1.982	2.01	8.2	8.2	2.35
360	1.982	1.982	2.01	8.2	8.2	2.35

*Most of the simulated spectrum agreed well with the observed spectrum as shown in **Fig. 6c**.

Table S6. The parameters for reproducing the main peak at different magnetic-filed-angles (θ/°) for the *c*-axis rotation spectra at 143 K.*

θ/°	g_x	g_y	g_z	Γ_x (mT)	Γ_y (mT)	Γ_z (mT)
0	1.999	1.999	2.008	2.39	2.39	2.24
30	2.001	2.001	2.0105	2.79	2.79	2.6
60	2.0005	2.0005	2.0123	2.85	2.85	2.4
90	2.001	2.001	2.011	2.95	2.95	1.9
120	1.999	1.999	2.007	1.9	1.9	1.6
150	1.998	1.998	2.007	2.95	2.95	1.7
180	2	2	2.009	2.95	2.95	1.75
210	2.001	2.001	2.012	2.95	2.95	1.75
240	2.0007	2.0007	2.013	3	3	1.75
270	1.999	1.999	2.01	3	3	1.98
300	2	2	2.007	3	3	2.2
330	1.998	1.998	2.006	3	3	2.2
360	1.998	1.998	2.007	3	3	2.2

*Most of the simulated spectrum agreed well with the observed spectrum as shown in **Fig. 6c**.

Table S7. The parameters for reproducing the main peak at different magnetic-filed-angles (θ/°) for the *c*-axis rotation spectra at 133 K.*

θ/°	g_x	g_y	g_z	Γ_x (mT)	Γ_y (mT)	Γ_z (mT)
0	1.999	1.999	2.008	2.39	2.39	1.5
30	2.001	2.001	2.009	2.39	2.39	2.29
60	2.0011	2.0011	2.009	2.32	2.32	2.43
90	2.0011	2.0011	2.009	2.32	2.32	2.05
120	2.0002	2.0002	2.007	2.32	2.32	1.7
150	1.999	1.999	2.007	2.32	2.32	2
180	2	2	2.0078	2.32	2.32	1.95
210	2.0008	2.0008	2.0099	2.32	2.32	2.06
240	2.0008	2.0008	2.0099	2.32	2.32	2.06
270	2.0005	2.0005	2.009	2.32	2.32	2.01
300	2.0005	2.0005	2.007	2.32	2.32	2.25
330	1.999	1.999	2.007	2.32	2.32	2.32
360	1.999	1.999	2.008	2.32	2.32	2.42

*Most of the simulated spectrum agreed well with the observed spectrum as shown in **Fig. 6c**.

Table S8. The parameters for reproducing the main peak at different magnetic-filed-angles (θ/°) for the *c*-axis rotation spectra at 123 K.*

θ/°	g_x	g_y	g_z	Γ_x (mT)	Γ_y (mT)	Γ_z (mT)
0	1.998	1.998	2.006	2.03	2.03	2
30	2.001	2.001	2.01	2.03	2.03	2
60	2.0015	2.0015	2.01	2.03	2.03	2
90	2.001	2.001	2.01	2.03	2.03	1.85
120	2.0007	2.0007	2.006	2.03	2.03	1.85
150	1.999	1.999	2.005	2.03	2.03	1.85
180	1.999	1.999	2.0065	2.03	2.03	1.85
210	2.0007	2.0007	2.009	2.03	2.03	1.85
240	2.0015	2.0015	2.0099	2.03	2.03	1.85
270	2.0005	2.0005	2.0095	2.03	2.03	1.85
300	2.0005	2.0005	2.0055	1.81	1.81	2.35
330	1.998	1.998	2.0055	1.6	1.6	1.65
360	1.999	1.999	2.0059	1.65	1.65	1.85

*Most of the simulated spectrum agreed well with the observed spectrum as shown in **Fig. 6c**.

Table S9. Best-fitting parameters in Eq. 2* for reproducing the observed θ-dependencies of g_x-values at different temperatures for the *b*-axis rotation spectra (Fig. 7).

T (K)	*A*	*a*	δ_1 (rad)	*B*	*b*	δ_2 (rad)	*C*
296	0.016346	0.017557	-1.4487	0.005278	-0.035239	2.6742	1.976
143	0.015078	0.015713	-1.429	0.019092	0.0349	-0.97513	1.9551
133	0.0092376	0.017453	-1.309	0.0053333	0.034907	-1.0472	1.9674
123	0.017511	0.017416	-1.5642	0.0066815	0.034631	-1.5213	1.9656

$*\chi_s(\theta)$ *or* $g_i(\theta) = Asin^2(a\theta + \delta_1) + Bsin^2(b\theta + \delta_2) + C,\ (i = x, y, z)$

Table S10. Best-fitting parameters in Eq. 2* for reproducing the observed θ-dependencies of g_y-values at different temperatures for the *b*-axis rotation spectra (Fig. 7).

T (K)	*A*	*a*	δ_1 (rad)	*B*	*b*	δ_2 (rad)	*C*
296	0.025667	0.017745	1.5189	0.0028142	-0.03971	-0.8746	2.0218
143	0.013121	0.015713	1.5525	0.010439	0.0349	-1.085	2.0161
133	0.01686	0.017926	1.2989	0.0071688	0.0339	-0.91384	2.0186
123	0.018935	0.01649	1.7441	0.0046186	0.0055733	2.1382	2.0239

$*\chi_s(\theta)$ *or* $g_i(\theta) = Asin^2(a\theta + \delta_1) + Bsin^2(b\theta + \delta_2) + C,\ (i = x, y, z)$

Table S11. Best-fitting parameters in Eq. 2* for reproducing the observed θ-dependencies of g_z-values at different temperatures for the *b*-axis rotation spectra (Fig. 7).

T (K)	*A*	*a*	δ_1 (rad)	*B*	*b*	δ_2 (rad)	*C*
296	0.011526	0.01749	1.7691	0.0053094	-0.03501	-0.5083	2.0315
143	0.04764	0.017249	1.6778	0.037737	-0.036094	2.8839	2.0789
133	0.046313	0.017259	1.6126	0.01948	-0.036293	2.6389	2.0667
123	0.064716	0.017464	1.5688	0.00043878	-0.0019695	3.4994	2.0678

$*\chi_s(\theta)$ *or* $g_i(\theta) = Asin^2(a\theta + \delta_1) + Bsin^2(b\theta + \delta_2) + C,\ (i = x, y, z)$

Table S12. Best-fitting parameters in Eq. 2* for reproducing the observed θ-dependencies of spin susceptibilities χ_s at different temperatures for the *b*-axis rotation spectra (Fig. 7).

T (K)	*A*	*a*	δ_1 (rad)	*B*	*b*	δ_2 (rad)	*C*
296	8.1999	0.017001	-1.7147	3.7935	-0.035296	2.2476	12.397
143	8.5936	0.017526	-1.7334	3.7197	-0.035112	3.6861	16.525
133	8.2938	0.017557	-1.7603	3.1706	-0.069647	-0.6267	15.783
123	7.1473	0.017242	-1.4331	5.0088	-0.034026	2.8542	16.48

$*\chi_s(\theta)$ *or* $g_i(\theta) = Asin^2(a\theta + \delta_1) + Bsin^2(b\theta + \delta_2) + C,\ (i = x, y, z)$

Table S13. Best-fitting parameters in Eq. 2* for reproducing the observed θ-dependencies of g_x-values at different temperatures for the *c*-axis rotation spectra (Fig. S2).

T (K)	*A*	*a*	δ_1 (rad)	*B*	*b*	δ_2 (rad)	*C*
296	0.0026563	0.015171	-1.1826	0.0028229	-0.013695	1.3252	1.9806
143	0.0028108	0.017603	2.1338	0.001487	-0.032032	-1.2829	2.0003
133	0.0023485	0.017509	1.9739	0.0010502	-0.035027	-0.6962	2.0008
123	0.0028008	0.018198	1.7697	0.0013858	-0.03559	-0.31621	2.0009

$*\chi_s(\theta)$ *or* $g_i(\theta) = Asin^2(a\theta + \delta_1) + Bsin^2(b\theta + \delta_2) + C,\ (i = x, y, z)$

Table S14. Best-fitting parameters in Eq. 2* for reproducing the observed θ-dependencies of g_y-values at different temperatures for the *c*-axis rotation spectra (Fig. S2).

T (K)	*A*	*a*	δ_1 (rad)	*B*	*b*	δ_2 (rad)	*C*
296	0.0026563	0.015171	-1.1826	0.0028229	-0.013695	1.3252	1.9806
143	0.0028108	0.017603	2.1338	0.001487	-0.032032	-1.2829	2.0003
133	0.0023485	0.017509	1.9739	0.0010502	-0.035027	-0.6962	2.0008
123	0.0028008	0.018198	1.7697	0.0013858	-0.03559	-0.31621	2.0009

$*\chi_s(\theta)$ *or* $g_i(\theta) = Asin^2(a\theta + \delta_1) + Bsin^2(b\theta + \delta_2) + C,\ (i = x, y, z)$

Table S15. Best-fitting parameters in Eq. 2* for reproducing the observed θ-dependencies of g_z-values at different temperatures for the *c*-axis rotation spectra (Fig. S2).

T (K)	*A*	*a*	δ_1 (rad)	*B*	*b*	δ_2 (rad)	*C*
296	0.0077549	0.017961	2.0427	0.0041656	-0.0078868	0.1412	2.0148
143	0.0064882	-0.017556	-2.1536	0.00077104	0.051054	0.88441	2.0122
133	0.0029475	0.01759	2.1978	0.00034484	0.037143	1.2966	2.0096
123	0.0056467	0.017425	2.0973	0.0011569	-0.039852	2.4484	2.0099

$*\chi_s(\theta)$ *or* $g_i(\theta) = Asin^2(a\theta + \delta_1) + Bsin^2(b\theta + \delta_2) + C,\ (i = x, y, z)$

Table S16. Best-fitting parameters in Eq. 2* for reproducing the observed θ-dependencies of spin susceptibilities χ_s at different temperatures for the *c*-axis rotation spectra (Fig. S2).

T (K)	*A*	*a*	δ_1 (rad)	*B*	*b*	δ_2 (rad)	*C*
296	8.1999	0.017001	-1.7147	3.7935	-0.035296	2.2476	12.397
143	8.5936	0.017526	-1.7334	3.7197	-0.035112	3.6861	16.525
133	8.2938	0.017557	-1.7603	3.1706	-0.069647	-0.6267	15.783
123	7.1473	0.017242	-1.4331	5.0088	-0.034026	2.8542	16.48

$*\chi_s(\theta)$ *or* $g_i(\theta) = Asin^2(a\theta + \delta_1) + Bsin^2(b\theta + \delta_2) + C,\ (i = x, y, z)$

References

S1 K. Bender, I. Hennig, D. Schweitzer, K. Dietz, H. Endres and H. J. Keller, *Mol. Cryst. Liq. Cryst.*, 1984, **108**, 359.